Applied Soft Computing Journal 99 (2021) 106874

Contents lists available at ScienceDirect

Applied Soft Computing Journal

journal homepage: www.elsevier.com/locate/asoc

A convolutional neural network model for abnormality diagnosis in a nuclear power plant

Gyumin Lee [a], Seung Jun Lee [b,*], Changyong Lee [c,*]

[a] School of Management Engineering, Ulsan National Institute of Science and Technology, 50 UNIST-gil, Ulsan 44919, Republic of Korea
[b] School of Mechanical, Aerospace and Nuclear Engineering, Ulsan National Institute of Science and Technology, 50 UNIST-gil, Ulsan 44919, Republic of Korea
[c] Graduate School of Management of Technology, Sogang University, 35 Baekbeom-ro, Mapo-gu, Seoul 04107, Republic of Korea

ARTICLE INFO

Article history:
Received 2 March 2020
Received in revised form 19 August 2020
Accepted 1 November 2020
Available online 11 November 2020

Keywords:
Nuclear power plant
Abnormality diagnosis
Convolutional neural network

ABSTRACT

Diagnosing abnormal events in nuclear power plants (NPPs) is a challenging issue given the hundreds of possible abnormal events that can occur and the thousands of plant parameters that require monitoring. This study proposes a convolutional neural network model for abnormality diagnosis in an NPP. The distinct feature of the proposed approach is the use of two-channel two-dimensional images to deal with (1) the massive amount of data that individual systems generate in real time, and (2) the dynamics of the states of individual systems. One channel represents the current NPP state values, while the other channel represents the changing patterns of the state values during a prescribed time period in the past. Experimental results from a full-scope simulator confirm, with statistically significant outcomes, that the developed model outperforms other classification models in terms of accuracy and reliability and is robust across different contexts of analysis, and thus has the potential to be adopted by actual NPP systems for real-time diagnosis.

1. Introduction

A nuclear power plant (NPP) is a large-scale complex system comprising thousands of individual systems (e.g. equipment and control systems), with safety given as the top priority [1]. Even though the damages caused by abnormal events in a plant may vary to a great extent, any such damages are likely to involve huge public and economic loss. When faced with an abnormal event, operators identify the causes of the current situation and perform corrective actions based on the abnormal operating procedures (AOPs) to return the plant to the normal condition [2]. If the situation is too severe to cope with via AOPs or becomes worse by improperly implemented AOP operations, the reactor is shut down and the plant transitions to a hot standby state, which is called an accident or emergency situation [3].

Most NPPs provide a large volume of AOPs with which operators are able to identify the list of actions to be done and the procedures to conduct them following the occurrence of an abnormal event. However, although the expected symptoms of abnormal events are described in the AOPs, event diagnosis is difficult even for well-trained operators since there are hundreds of possible related events that can occur and thousands of plant parameters that require monitoring [4]. For instance, the APR1400, which is the latest NPP developed in the Republic of Korea, has 82 different AOPs, each of which includes multiple sub-procedures representing different causes for a given system failure, many of which in turn require different corrective actions [5]. Moreover, many abnormal events present similar symptoms and involve multiple alarms, which can also affect each other [2]. Hence, some symptoms might not be clearly discerned in the AOPs.

These necessitate the development of systematic models and methods to reduce the time and effort associated with abnormality diagnosis in NPPs. Highlighting possible avenues for methodological adaptation, recent studies have developed data-driven approaches. For instance, Yao et al. [6] presented a fault diagnosis system for an NPP based on a state information-imaging method by applying kernel principal component analysis (KPCA) using data obtained from a full-scope simulator. Wang et al. [7] developed a fault diagnosis technique with regard to tiny leakages in pipelines in an NPP, based on an integration of knowledge-based and data-driven methods using sample data containing major plant parameters extracted from a full-scope simulator. Tolo et al. [8] proposed an on-line diagnosis tool to identify the severity of a loss of coolant accident (LOCA) in NPPs based on the combination of a set of artificial neural networks (ANNs) that enhances robustness and quantifies the confidence bounds associated with the prediction. Pinheiro et al. [9] suggested an

* Corresponding authors.
E-mail addresses: optimist@unist.ac.kr (G. Lee), sjlee420@unist.ac.kr (S.J. Lee), changyong@sogang.ac.kr (C. Lee).

https://doi.org/10.1016/j.asoc.2020.106874
1568-4946/

approach to provide "don't know" response capability to a deep learning-based system for the NPP accident identification problem by employing several data-driven methods, such as a particle swarm optimisation (PSO), autoencoder (AE), and deep one-class autoencoder (DOCAE).

However, while previous data-driven approaches have proved quite useful for detecting transients or faults that can lead to accidents (e.g. LOCA or steam generator tube rupture), they are not effective in diagnosing abnormal events as specified in AOPs because these approaches use a limited number of plant parameters for specific individual systems. Accidents, in many cases, present more specific symptoms and have fewer types than abnormal events, and thus can be identified by dozens of key plant parameters. On the contrary though, the number of plant parameters that should be monitored for abnormal event diagnosis is over a thousand because of the large number of abnormal events that can occur and the high variety of causes and symptoms. Hence, previous individual system-level analysis should be extended into plant-level analysis. Another consideration is associated with the dynamics of NPP states: as the states of individual systems in an NPP change from moment to moment, the differences in state values between timestamps can provide clues for diagnosing abnormal events [10]. Despite this, most previous approaches are not effective in modelling such dynamic aspects. In particular, the computational complexity and cost associated with existing approaches escalate sharply if dynamic aspects of individual systems are incorporated into abnormality diagnosis at the plant-level.

To solve these problems, we develop a convolutional neural network (CNN) model for abnormality diagnosis in an NPP. CNN is one of the derivatives of deep neural networks inspired by the workings of the visual processing system in the human brain, which only responds to its local receptive field [11]. The network has shown considerable success in image analysis tasks including facial recognition [12,13], handwritten character recognition [14], image semantic segmentation [15], and medical image classification [16,17]. The premise of the current research is that CNNs, with their ability to deal with image data, can be effective in handling the massive amount of plant data generated in real time and diagnosing abnormal events, if the data is properly converted into an image format. Building on this notion, the proposed approach adopts two-channel two-dimensional (2D) images to describe NPP state values. Specifically, one channel represents the current NPP state values, while the other channel represents the changing patterns of the NPP state values during a prescribed time period in the past. Consequently, the model is designed to deal with (1) the massive amount of data that individual systems generate, and (2) the dynamics of the states of individual systems.

The proposed approach was applied to data generated by a full-scope simulator. By imitating NPP operation, full-scope simulators are capable of generating operating history data almost similar to a real NPP, and they have been widely used for the training of NPP operators in practice [18,19]. Moreover, while abnormal events rarely occur in the real world [20], the data describing NPP state values under abnormal events can be obtained as many as needed by setting up malfunctions in the simulator. Thus, it is considered reliable and practical to use the data generated by the full-scope simulator for abnormality diagnosis in an NPP. Experimental results confirm, with statistically significant outcomes, that the proposed approach outperforms other classification models (namely one-channel CNN, ANN, PCA+ gated recurrent unit (GRU), and support vector machine (SVM)) in terms of accuracy and reliability. The proposed model is also considered robust across different analysis contexts and thus has the potential to be adopted by actual NPP systems for real-time diagnosis.

The remainder of this paper is organised as follows. Section 2 introduces related work on the diagnosis of abnormal events in an NPP. Section 3 details the proposed approach, and Section 4 presents the experimental settings employed in this study. Section 5 reports the performance of the developed model with other classification models. Section 6 discusses its related practicality as a tool for real-time abnormality diagnosis in an NPP. Section 7 presents our conclusions.

2. Related work

Over the past few decades, a variety of models and methods have been proposed to identify the abnormal events in NPPs, which can mainly be classified into model-based and data-driven approaches. The model-based approaches in general identify abnormal events based on abnormal changes in the residuals, meaning the differences between actual observation and the analytically calculated values of plant parameters by a mathematical model [21,22]. These model-based approaches have demonstrated their usefulness for the identification of abnormal events in NPPs by adopting various methods including the sequential probability ratio test (SPRT) [23], neuro-fuzzy networks [24], or singular-value decomposition (SVD) [25]. However, such approaches have difficulties to be applied in practice due to their low performance with complex systems as well as a lack of robustness in covering a variety of abnormal events [26].

On the other hand, the data-driven approaches based on pattern recognition-related algorithms have been presented as alternatives to the model-based approach. Data-driven approaches basically try to find the relationships between plant parameters and abnormal events using multivariate statistical methods or machine learning techniques. As one of the earliest studies, Horiguchi et al. [27] diagnosed 100 causes of abnormality by using patterns of 49 plant parameters in the training of an ANN. Similarly, Santosh et al. [28] examined several optimisation algorithms for an ANN in order to diagnose four representative transient initiating events, such as moderator heat exchanger tube failure and shutdown cooling heat exchanger tube failure, by employing reactor operating parameters in the NPP as independent variables for prediction. Zio [29] proposed a hierarchical SVM structure consisting of a one-class SVM and multi-class SVM for transient classification in NPP systems. It uses NPP simulator signals as its input data and predicts five anomaly classes derived from a transient regarding faults in line 1 of an NPP feedwater system. In addition, Galbally and Galbally [30] developed a dynamic time warping (DTW) algorithm-based system for the automatic classification of nine plant transients, such as reduction to 0% power or shut down vessel flooding, through the use of seven plant parameters and boundary conditions extracted from real operational data of the Cofrentes NPP.

More recently, several improved methodologies have been proposed by combining multiple machine learning algorithms or adopting deep learning methods in order to handle more accurate judgements for various diagnostic situations. In Ayodeji et al. [31], a knowledge base for an NPP operator support system was presented based on fault diagnosis using PCA and two different recurrent neural networks—the Elman neural network (ENN) and the radial basis network (RBN). They used eight plant parameters provided by the Qinshan II NPP simulator to diagnose five faults including steam generator tube rupture and locked rotor fault. Specifically, the PCA was utilised for filtering noise and reducing the dimension of the plant parameters, and the recurrent neural networks were utilised for predicting two output values indicating the location and the size of each fault. Peng et al. [32] suggested a fault diagnosis method to deal with seven types of representative accidents in an NPP, such as LOCA, steam line

break, or load rejection. They used 36 plant parameters related to pressure, temperature, or water level obtained from the PCTRAN NPP simulator, and employed correlation analysis as a dimensionality reduction method and a deep belief network (DBN) as a classifier for fault identification. Wang et al. [7] presented a fault diagnosis technique for NPPs that provides high detection accuracy with a small number of samples by the integration of knowledge-based and data-driven methods using SVM and PSO. They collected sample data with major plant parameters from a full-scope simulator for model training and testing with the aim to identify small faults in an NPP such as a small leakage in the cold leg of the reactor coolant system. Yao et al. [6] proposed a new approach for a fault diagnosis system in an NPP based on a state information-imaging method by applying KPCA as a feature extractor and five basic machine learning algorithms, namely SVM, K-nearest neighbour (KNN), linear discriminant analysis (LDA), decision tree (DT), and logistic regression (LR), as the classifier. They utilised a total of 316 plant parameters obtained from a full-scope simulator of the China Lead-based Research Reactor (CLEAR). Kim et al. [33] also suggested an abnormality diagnosis system for determining several abnormal events and their detailed causes related to the AOPs of the APR-1400 on the basis of PCA and two-stage gated recurrent unit (GRU). They extracted 20 features by reducing the dimension of about 1000 plant parameters through the PCA and used them as inputs to the GRUs.

In line with such studies, some researchers especially focused on the additional issues that have to be considered for abnormality diagnosis, such as measuring the severity of an accident or dealing with unknown or "don't know" types of abnormal events. Tolo et al. [8] measured the severity of LOCA in NPPs based on the combination of a set of ANNs that takes several sources of input uncertainty (e.g. data noise or model uncertainty) into account. Nicolau and Schirru [34] presented a methodology on the basis of the quantum evolutionary algorithm (QEA) for the nuclear accident identification problem that is able to distinguish unknown types of accidents from other known accidents in training scope. Pinheiro et al. [9] suggested auxiliary methods to supply a previously developed deep neural network-based system for abnormality diagnosis in NPPs with the ability to generate a "don't know" response by applying several algorithms including PSO or AE.

These recently developed data-driven approaches have contributed to the research on NPP abnormality diagnosis as they allow us to utilise vast amounts of data obtained from NPP systems and identify transients or faults of the systems quicker than human operator judgement. Nevertheless, the approaches have certain limitations as stated in Section 1. These provide the underlying motivation and are addressed in this study.

3. Methodology

The overall process of the proposed approach consists of four stages, as covered in this section. First, the data generation process for collecting raw data from an NPP simulator is described. Second, the data transformation process is detailed, involving the conversion of raw data into two-channel 2D image data that represents the NPP state values at a certain time and their changing patterns. Third, as the main part of the methodology, abnormality diagnosis via CNN is described in detail. Finally, performance evaluation is introduced with four quantitative evaluation metrics for measuring the performance, reliability, and practicality of the developed model.

3.1. Data generation

Abnormal situations can be demonstrated by setting up malfunctions provided in the simulator. A Python programme was developed to automate the data collection process, as described below.

- Step 1: Load the initial condition of a plant. Here, the initial condition is the normal condition in which the plant operates at 100% power generation without any events. In this study, only 100% operating normal condition is considered as the initial condition, yet other initial conditions (e.g. startup and shutdown operation) can be added by further simulations for a more robust diagnosis.
- Step 2: Set up malfunctions corresponding to the target abnormal event. A malfunction represents a predefined failure of a component, such as a stuck-open failure of a valve, abnormal stop of a pump, or leakage of a pipe. Here, we can model different scenarios for a malfunction by adjusting the final value of malfunction severity and the amount of time during which time the malfunction variable gradually changes from the current value to the final value. Also, there is a possibility that the power generated by the plant is reduced to less than 100% depending on the malfunction injected.
- Step 3: Define the plant parameters to be monitored. The parameters describe the NPP state values, which include temperature, pressure, and flow rate, and the states of the components such as valves and pumps.
- Step 4: Run the simulator. Here, the NPP state values are accumulated once per timestamp, usually at 1 s intervals.
- Step 5: Freeze the simulator after the designated period.
- Step 6: Save and export the NPP state values after one abnormal event simulation.

This programme has been utilised in the previous study that suggested an abnormality diagnosis system employing PCA and GRU at the same time [33].

3.2. Data transformation

The data obtained in the previous step includes more than a thousand variables corresponding to NPP state values. The use of such a large number of variables in building a classification model not only results in long training times but also requires a huge number of training samples [35,36]. Several recent studies have attempted to remedy these shortcomings by representing their high dimensional data as images to be used as inputs to a CNN model [37–39]. The structure of CNNs reduces the number of parameters to be updated by performing convolution and pooling operations, thereby effectively dealing with high dimensional data with advantages in saving computational cost and time. Based on this technique, the approach developed here employs image data that describe the NPP state values at a certain point in time and also the changing patterns of NPP state values during a prescribed time period in the past.

The detailed process of data transformation from raw data into two-channel 2D images is presented as follows. First, as the ranges of the variables in the raw data vary from one to another, the data needs to be normalised. We utilise the min–max feature scaling method to normalise the data based on the minimum and maximum values of each variable obtained from the NPP simulator, as formulated by:

$$X_{\text{normalised}} = \frac{X - X_{\min}}{X_{\max} - X_{\min}} \tag{1}$$

The maximum and minimum values of each variable (i.e. plant parameter) are predefined according to the upper and lower bounds of the variable derived from the simulation formulas. Thus, the maximum and minimum values are applied globally across all data samples, and the data generated from the simulator in principle do not contain any values outside the specified range [40]. Consequently, we can differentiate two such scenario data that show the same tendency but have differences in the values via the global minimum and maximum values. Second, the normalised scenario data is transformed into a set of square 2D images. Generally, square 2D images can be more readily handled than rectangular 2D images. In the case where the number of variables in the data is not a square number, adding some zero values enables the data to be converted into a square shape, as shown in Fig. 1; we note that such a zero-padding scheme does not affect the performance of the classification model since it merely adds some dummy information to the data [41]. Third, the changes in the NPP state values during a prescribed time period in the past (i.e. time-lag) are captured and converted into a 2D image in the same manner as above. Examples of these converged 2D images are presented in Fig. 2(a) and (b). Finally, the two 2D images generated in the second and third steps are overlapped to construct a two-channel 2D image data, as illustrated in Fig. 2(c). The images are presented in grey scale, where black and white pixels indicate zero and one, respectively; here, the images in Fig. 2 were created using Python library Matplotlib by setting the colour map to grey scale and 0–1 as the range that the colour map covers [42]. The procedure is repeated every timestamp from a point in time after the first prescribed time period to the end of the designated period to generate two-channel 2D image data samples used as inputs to the classification model for abnormality diagnosis.

3.3. Abnormality diagnosis via CNN

The CNN model employed in this study consists of two parts, feature extraction and classification, as depicted in Fig. 3. Once the two-channel 2D image data is fed as an input, a series of layers (i.e. convolution layers and pooling layers) construct feature maps from the input data. Second, a fully connected layer then flattens the constructed feature maps and computes classification scores for each type of abnormal event. The structure of the proposed CNN model is presented in detail, as follows.

3.3.1. Convolution layer

The convolution layer accepts images from the previous layer (i.e. input images) and constructs feature maps through a convolution operation that applies trainable filters across the transferred image. Filters in the convolution layers are a square matrix of a certain size consisting of weights to be updated during the training process. Each filter shares weights and performs a convolution operation by sweeping through the image transferred from the previous layer, multiplying the matrix corresponding to each element of the image, and adding them together. In the convolution operation, the size of the feature maps to be constructed is determined by the size of the filter, and the depth (i.e. the number of channels) of the feature maps is decided by the number of filters corresponding to the number of channels in the convolution layer.

Fig. 4 displays an example of the convolution operation consisting of three components assumed to be a square matrix: input image, filter, and output image. In Fig. 4, the input image is represented as $I \in \mathbb{R}^{M_i \times N_i}$, where M_i and N_i indicate the sizes of the input image, which are the number of rows and columns, respectively. Likewise, the output image (i.e. feature map) is represented as $O \in \mathbb{R}^{M_o \times N_o}$, where M_o and N_o indicate the size of the output image. The filter is expressed as $F \in \mathbb{R}^{M_f \times N_f}$, where F indicates the size of the filter. Then, the output value is calculated as Eq. (2):

$$o(m_o, n_o) = \sum_{m_f=0}^{M_f} \sum_{n_f=0}^{N_f} f(m_f, n_f) \cdot i(m_i + m_f, n_i + n_f), \ where$$
$$m_o = 0, 1, \ldots, M_o; n_o = 0, 1, \ldots, N_o;$$
$$m_i = 0, 1, \ldots, M_i; n_i = 0, 1, \ldots, N_i, as\ indexes \quad (2)$$

In the equation, $o(\cdot, \cdot)$ is each value of the output image, $f(\cdot, \cdot)$ is each weight of the filter, and $i(\cdot, \cdot)$ is each value of the input image. Each filter sweeps the input image with a certain amount of stride, and thus the size of the output image is naturally determined by:

$$M_o = \frac{(M_i - M_f)}{S} + 1; N_o = \frac{(N_i - N_f)}{S} + 1, where\ S\ is\ stride \quad (3)$$

In general, the output of each convolution layer passes through an activation function in order to give non-linearity to the network before entering the next layer. For this, we employ a rectified linear unit (ReLU) as the nonlinear activation function, as formulated in Eq. (4):

$$f(x) = \max(0, x) \quad (4)$$

3.3.2. Pooling layer

A pooling layer conducts down-sampling to reduce the spatial size of the feature maps, thereby decreasing the number of parameters and preventing overfitting. This layer utilises a filter in a similar manner to the convolution layer, but the filter in the pooling layer differs in that it resizes the image spatially without any weight to be trained. There are two typical types of pooling operation, namely max pooling and average pooling. Max pooling chooses the maximum value in a sliding window, while average pooling takes the average value over the sliding window. As mentioned in Section 3.2, the second channel of the two-channel 2D image represents the amount of changes in the NPP state values during a prescribed time period. Generally though, NPP state values rarely change in the normal state and only a few plant parameters show fluctuation even in an abnormal state. That is, most values of such images are close to zero, except for a few large values. In this context, we employ max pooling for better capturing the change in state values since average pooling can cause substantial information loss [43]. With the max pooling operation, applying a 2×2 filter with a stride of 2, for example, will result in 75% of the values of the input image being discarded. Then, the remaining values (i.e. maximum values in each sliding window) are delivered into the next layer.

3.3.3. Fully connected layer

A fully connected layer usually serves as the last hidden layer in a CNN and carries out a classification task using the feature maps extracted from the previous layers. After several convolution and pooling layers, the 2D feature maps are firstly flattened into a one-dimensional vector as an input to be connected to the last layer. Subsequently, the fully connected layer computes a classification score for each output (i.e. the predicted probabilities for each abnormal event and normal state in an NPP) through a matrix multiplication of the feature maps and weights in the layer, in the same manner as the hidden layers of a traditional artificial neural network. Here, a softmax function is used as the activation function in this layer for converting the output values into a probability distribution over the predicted labels, as formulated in Eq. (5):

$$f(x_i) = \frac{exp(x_i)}{\sum_{i=0}^{k} \exp(x_i)}, \ where\ i = 0, 1, \ldots, k \quad (5)$$

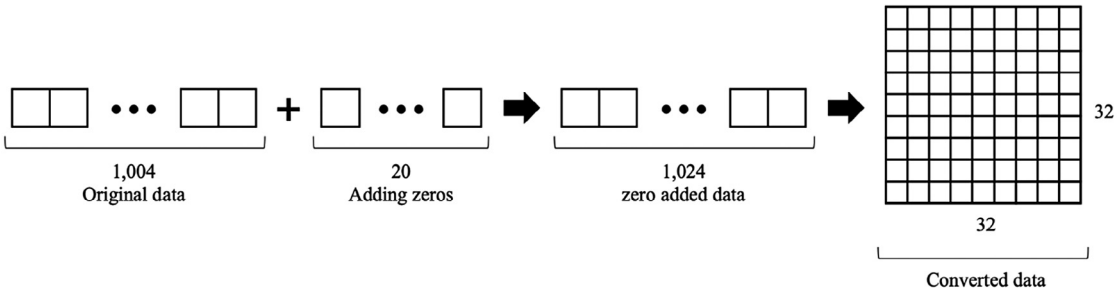

Fig. 1. Example of adding zeros.

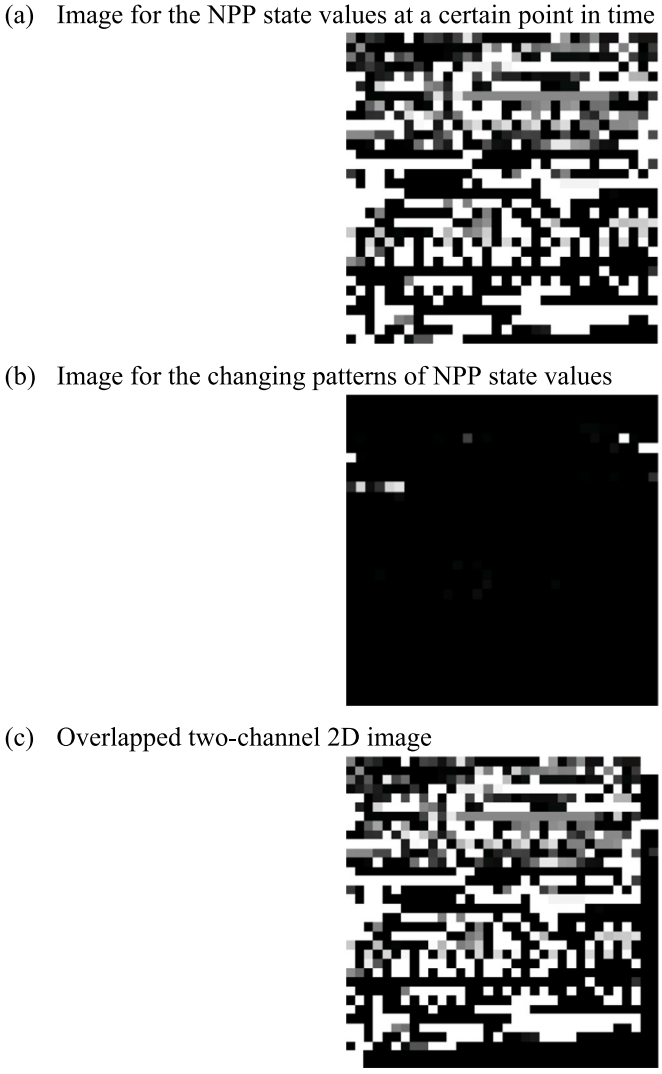

Fig. 2. Example of the result of data transformation. (a) Image of the NPP state values at a certain point in time. (b) Image of the changing patterns of NPP state values (c) Overlapped two-channel 2D image.

3.4. Performance evaluation

Considering that abnormality diagnosis in an NPP is a multi-class classification problem, several performance evaluation metrics are examined to assess the performance of our approach after a confusion matrix is constructed. First, we measure the accuracy per class and the overall accuracy of the developed model as defined in Eqs. (6) and (7) [44,45]:

$$\text{Accuracy}_i = \frac{tp_i + tn_i}{fp_i + fn_i + tp_i + fn_i} \tag{6}$$

$$\text{Overall accuracy} = \frac{\sum_{i=1}^{l} \frac{tp_i + tn_i}{fp_i + fn_i + tp_i + fn_i}}{l} \tag{7}$$

Here, true positive (tp_i), true negative (tn_i), false positive (fp_i), and false negative (fn_i) for class i represent, respectively, the number of positive examples correctly classified, the number of negative examples correctly classified, the number of negative examples wrongly classified as positive, and the number of positive examples wrongly classified as negative. The number of classes is l.

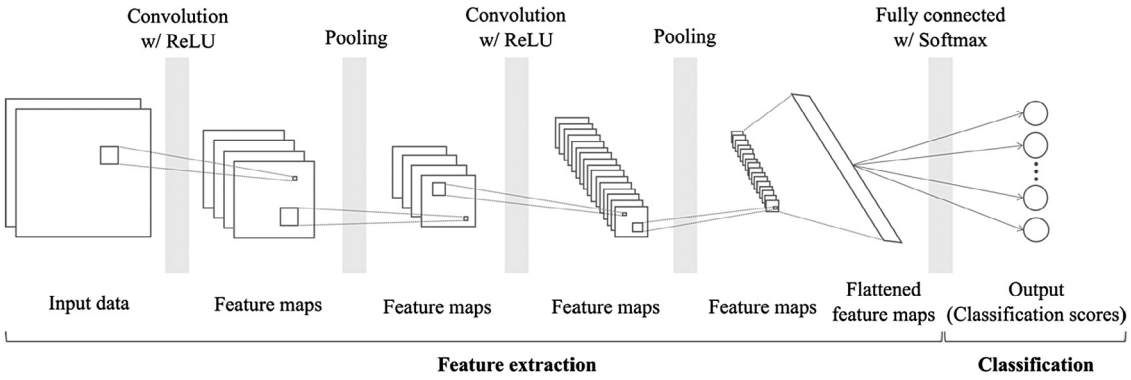

Fig. 3. Overall structure of the proposed CNN model.

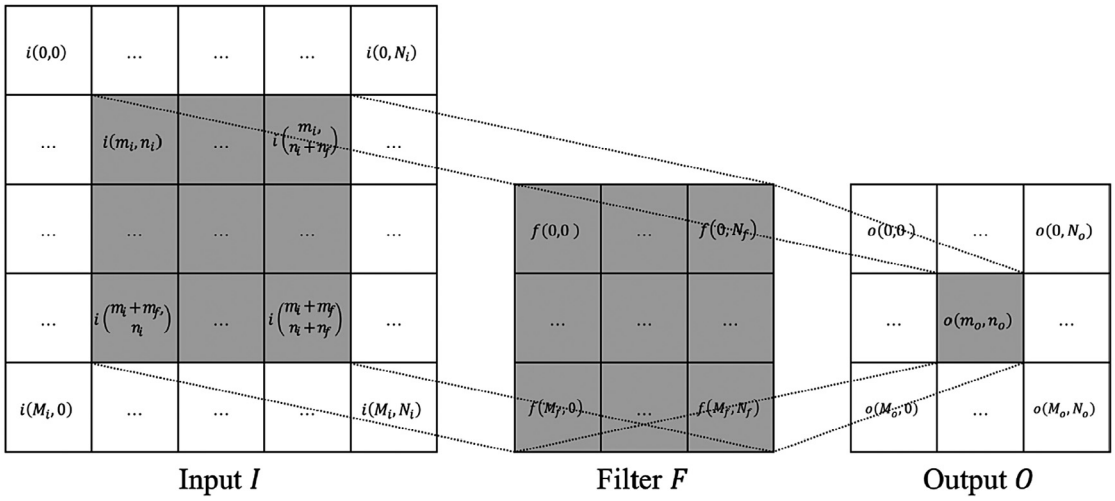

Fig. 4. Example of the convolution operation.

Second, we calculate precision, recall, and F1 score to assess reliability and practicality [46]. Precision is the fraction of true positive results among all results classified as positive, as in Eq. (8), while recall is the fraction of true positive results among the results that should have been returned, as in Eq. (9). Typically, a high precision value indicates that the classification result is consistently reliable, while a high recall value represents that the model has a lower risk of misclassifying the positive events. Lastly, the F1 score is a measure of the general effectiveness of the model with respect to the classification of positive events, defined as the harmonic average of precision and recall, as in Eq. (10). Values in this measure range between 0 (poor classification) and 1 (perfect classification). The overall measure of these metrics can also be calculated in the same way as the overall accuracy.

$$\text{Precision}_i = \frac{\text{tp}_i}{\text{tp}_i + \text{fp}_i} \tag{8}$$

$$\text{Recall}_i = \frac{\text{tp}_i}{\text{tp}_i + \text{fn}_i} \tag{9}$$

$$\text{F}_1\ \text{score} = 2 \cdot \frac{precision \cdot recall}{precision + recall} \tag{10}$$

4. Experimental setting

4.1. Data

This study used a 3KEYMASTER full-scope simulator for data collection. This simulator is designed for a generic 1400 MWe pressurised water reactor, named the Advanced Power Reactor 1400 (APR-1400) that is currently in operation in Shin Kori units 3 and 4 in the Republic of Korea, and includes (1) primary, (2) secondary, and (3) support and safety systems [19,33,40]. Accordingly, the simulator covers almost all components and functions of the real NPP systems, with the symptoms and conditions of simulated abnormal operating scenario matching those based on the AOPs of the real NPP. Moreover, the simulator meets the requirements of "Nuclear power plant simulators for use in operator training and examination" from the American National Standards Institute (ANSI) [47] and thus has been used to train NPP operators to handle abnormal events that rarely occur in the real NPP [19,20]. Therefore, the model developed using the data generated by the simulator can be deployed in practice. In the process of data collection, the developed Python programme mentioned in the previous section was used; while no licence is required to use the programme, it is not publicly available in practice since the programme only works in conjunction with the simulator, which is commercialised.

In addition to the normal state, a total of 10 abnormal events were selected to cover the entire scope of the NPP, as shown in Fig. 5. The chosen events are considered more significant than others in terms of occurrence probability or consequence; descriptions of the abnormal events are summarised as follows.

(1) Primary system abnormalities:

- POSRV: Leakage of the pilot-operated safety relief valve that depressurises the reactor coolant system;
- LTDN: Abnormality in the letdown water system that controls the reactor coolant system inventory;

- CHRG: Abnormality in the charging water system that controls the reactor coolant system inventory;
- RCP: Abnormality in the reactor coolant pumps that circulate coolant in the primary system.

(2) Secondary system abnormalities:

- SGTL: Leakage of tubes inside steam generators;
- CDS: Abnormality in the condenser vacuum for the cooling steam transferred from the steam generators;
- MSS: Abnormality in the main steam system that provides steam to the turbines;
- CWS: Abnormality in the circulating water system that filters water before it is pumped to and through the condenser.

(3) Support and safety system abnormalities:

- RMW: Valve abnormality in the reactor makeup water tank that provides coolant to the volume control tank in emergency situations;
- MSIV: Abnormality in the main steam isolation valve that isolates the main steam in emergency situations.

In particular, the chosen abnormal events can be caused by a wide range of components in an NPP, rather than being closely connected to some specific system. Therefore, we utilised a total of 1004 plant parameters covering almost all components of NPP in order to deal with these events simultaneously. By and large, the plant parameters have different trends of values depending on the state of the NPP. As an example, by following the data generation and transformation procedures in Sections 3.1 and 3.2, we visualised the changing patterns of NPP state values under Normal state, LTDN and CHRG abnormal event scenarios 10 s after the simulation started, as shown in Fig. 6(a)–(c). While NPP state values hardly change under the Normal state, there exist several plant parameters that change significantly under the LTDN and CHRG events. For instance, the two prominent consecutive pixels on the upper left of Fig. 6(b) correspond to the plant parameters related to speed sensors, named 'TCSST1D' and 'TCSST1E', and the light grey pixel on the upper right corner of Fig. 6(c) corresponds to the plant parameter related to a departure from nucleate boiling ratio channel, named 'RPS_04_C'. Such differences can be the basis for the proposed model to identify each abnormal event at the model training stage.

As stated earlier, the trend of the NPP state values for each scenario varies depending on the severity of the abnormal event and the time the abnormality has been reached. For example, if the malfunction for the SGTL abnormal event is injected with the malfunction severity value of 0.1 and the ramp time of 10 s, the malfunction variable gradually changes from the initial condition to the 10% severe SGTL abnormal condition during 10 s. To construct a dataset describing different trends, the NPP simulator generated 300 different scenarios for each abnormal event with different combinations of the malfunction severity value in the range of 0.5% to 95% and the ramp time in the range of 10 s to 30 s. Accordingly, the dataset comprised 3300 total scenarios; here we used the same number of scenarios for each abnormal event and the normal state in order to avoid the imbalanced dataset problem that causes poor classification performance [32]. Each scenario included NPP state values during 30 s after the simulator started, with the 1004 numerical variables. Thus, all scenario data after generation have the shape of a $(30, 1004)$ matrix, in which each row represents the corresponding NPP state values at each timestamp (i.e. 1 s) after an abnormal event simulation. Then, each scenario data was normalised by the min–max feature scaling method, and transformed into a 32×32 2D images by adding 20 zeros to each row of the data. Finally, we set up 5 s as the time-lag value to obtain the changing patterns of NPP state values, and the two-channel 2D image data samples were constructed for each scenario data, by overlapping two images that describe the NPP state values at each timestamp and the changing patterns of NPP state values for 5 s. As a result, 25 $(=30-5)$ samples were drawn for each scenario data, and thus a total of 82,500 $(=3300 \times 25)$ samples were obtained for the entire dataset. These were used as the inputs of the proposed CNN model. Here, the time-lag value may affect the model performance. The shorter the time-lag is set, the greater the number of samples and the faster the diagnosis is, while the longer the time-lag is set, the longer it takes to diagnose and the smaller the number of samples is. However, the model with longer time-lag value may be advantageous for modelling the changing patterns of NPP state values since some plant parameters change slowly and many plant parameters affect each other. Thus, we investigate the effect of different time-lag values on the diagnostic performance of the proposed model through a further experiment in the following section.

For a thorough performance evaluation, we used the following model selection framework including dataset split and stratified k-fold cross validation. First, we left 10% of all samples out of the whole dataset for testing. Second, we applied stratified k-fold cross validation to the remaining 90% of the samples for hyper-parameter selection. In this step, the dataset was divided into k groups, and for each group, a model was trained by taking the remaining $k-1$ groups as training data and evaluated using the selected group as validation data. To avoid bias, in the first and second step we randomly sampled the data while maintaining the distribution of abnormal events. Finally, we adopted the best model, with the optimal combination of hyper-parameters based on the cross validation, and verified it using the remaining test dataset to obtain the final result of performance evaluation. Through this procedure, we can examine how the developed model performs in the scenarios never used in the training. Moreover, as the performance of the model is sensitive to the number of folds in the k -fold cross validation, we conducted a sensitivity analysis on the value of k from 5 to 10. There were no significant differences in the results over the six values of k, as reported in Appendix A. Accordingly, for the convenience of analysis, we determined 5 as the value of k for the cross validation.

4.2. Hyper-parameter selection

The proposed CNN model consists of two alternating convolution and pooling layers and one fully connected layer in order to conduct the feature extraction and classification tasks, with both pooling layers having a 2×2 pooling filter with a stride of 2. This model structure follows the standard CNN setup that has been confirmed to work well on a wide range of classification problems by several studies using data-driven approaches [48]. To ascertain the most suitable settings of the developed CNN model, hyper-parameters other than the size and stride of the pooling layer filters—namely, the number of filters in each convolution layer, the size of each convolution filter, and the number of neurons in the fully connected layer—were determined by a grid search experiment that explores how classification performance varies by different hyper-parameter values. First, candidates for the number of filters in the two convolution layers were set as three pairs: 8–16, 16–32, and 32–64 in the first and second convolution layers, respectively. Second, candidates for the size of the convolution filters were set to two square fields: 2×2 and 3×3 for each convolution layer. Lastly, candidates for the number of neurons in the fully-connected layer were set to 50 and 100. We built several CNN structures by applying every combination of the three hyper-parameters, trained them over

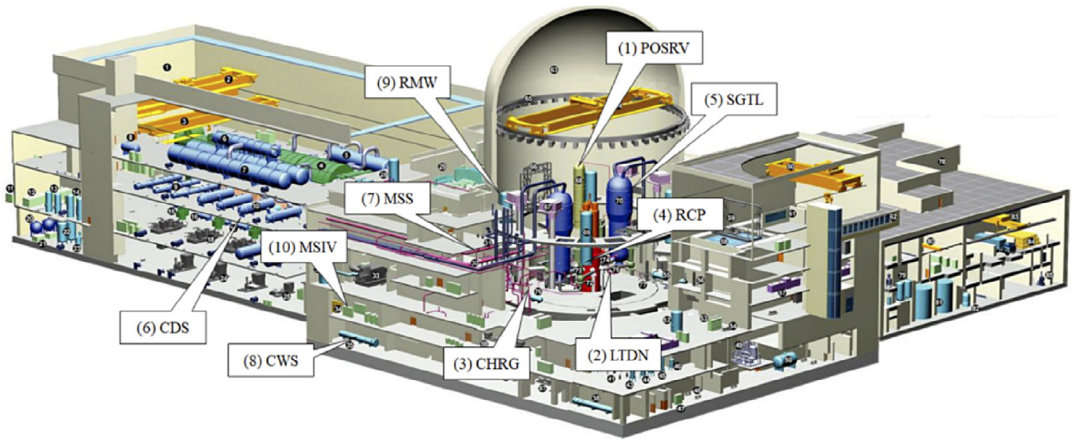

Fig. 5. Schematic diagram of the APR1400 with the locations of the ten selected system abnormalities.

Fig. 6. Images of the NPP state values under Normal, LTDN and CHRG scenarios. (a) Image of the changing patterns of Normal scenario at 10 s after the simulator started (b) Image of the changing patterns of LTDN scenario at 10 s after the simulator started (c) Image of the changing patterns of CHRG scenario at 10 s after the simulator started.

30 s with the data collected and transformed in the previous section, and obtained multiple classification performances with respect to the 5-Fold cross validation. With regard to a method for model training, generally the weights to be updated in each layer are estimated via backpropagation algorithms using a gradient descent method, which updates the weights by calculating the derivatives of a loss function with respect to the weights of the network. Specifically, we used categorical cross entropy as the loss function and the adaptive moment estimation (Adam) algorithm, which is known as an extension of the stochastic gradient descent method, as an optimiser for updating weights [49]. Results of the hyper-parameter selection process are presented in Table 1. Although there were no notable differences among the 12 total combinations of hyper-parameters, the CNN structure that applied 32–64 as the number of filters in the two convolution layers, 2×2 as the size of the convolution filters, and 100 as the number of neurons in the fully-connected layer showed the highest averaged classification performance metrics for the validation dataset. Hence, in the following comparative analysis and robustness test, the model with the best combination of the hyper-parameters identified through the cross validation was used.

5. Results

According to the experimental settings specified in Section 4, we conducted a comparative analysis between the two-channel CNN model and other major classification models used in previous studies, namely one-channel CNN, ANN [1,27,28,50], PCA+GRU [33], and SVM [29,51] to evaluate the performance of the developed model. For a fair comparison, the one-channel CNN was constructed in the same manner as the developed CNN model, except that it employed one-channel 2D images describing the current NPP state values as its input data. The ANN was developed after the network structure of [1] as its results show adequate performance. Similar to [33], a PCA+GRU method was constructed with the PCA acting as the feature extractor and the GRU acting as the classifier. In particular, GRU requires sequential data of a certain length, so its sequence length is set to 5 to employ the samples composed of 5 s intervals from each scenario data as its input. The SVM tested in this study was based on [51], except that here we applied the one-against-one method to implement multi-class classification [29]. For fair hyper-parameter selection and performance evaluation, we applied the same model selection and training framework to the aforementioned five classification models. Particularly in the dataset split and cross validation process, we set the same random state value for the random sampling so that the training, validation, and test dataset have the same distribution for every model. By the aforementioned model selection framework, we explored various configurations of the latter three models and selected the hyper-parameters that showed their best performances: five hidden layers of 128, 128, 64, 32, and 16 neurons in the ANN, one layer of 100 neurons in the GRU, and the radial basis function kernel in the SVM. During model training, we noticed that the SVM took 10 to 20 times longer to learn than other models, and thus we concluded that it was unrealistic to train it with the entire set of samples. Accordingly, for training the SVM,

Table 1
Results of the hyper-parameter selection process.

Number of filters in the first layer	Number of filters in the second layer	Filter size	Number of neurons in the FC layer	Accuracy	Precision	Recall	F1 score
8	16	2	50	0.9992	0.9960	0.9959	0.9959
8	16	2	100	0.9987	0.9933	0.9931	0.9931
8	16	3	50	0.9982	0.9906	0.9900	0.9900
8	16	3	100	0.9977	0.9882	0.9874	0.9875
16	32	2	50	0.9991	0.9949	0.9948	0.9948
16	32	2	100	0.9986	0.9926	0.9923	0.9924
16	32	3	50	0.9991	0.9952	0.9950	0.9950
16	32	3	100	0.9987	0.9929	0.9927	0.9927
32	64	2	50	0.9992	0.9959	0.9958	0.9958
32	**64**	**2**	**100**	**0.9993**	**0.9961**	**0.9960**	**0.9960**
32	64	3	50	0.9987	0.9930	0.9927	0.9927
32	64	3	100	0.9989	0.9940	0.9938	0.9938

Table 2
Performance evaluation metrics for the developed two-channel CNN.

Class	Accuracy	Precision	Recall	F1 score
Normal	0.9981	0.9791	1.0000	0.9894
SGTL	0.9994	1.0000	0.9933	0.9967
CHRG	0.9994	0.9934	1.0000	0.9967
LTDN	1.0000	1.0000	1.0000	1.0000
CDS	1.0000	1.0000	1.0000	1.0000
POSRV	1.0000	1.0000	1.0000	1.0000
RMW	0.9992	1.0000	0.9907	0.9953
CWS	0.9996	1.0000	0.9960	0.9980
MSIV	1.0000	1.0000	1.0000	1.0000
RCP	0.9993	1.0000	0.9920	0.9960
MSS	1.0000	1.0000	1.0000	1.0000
Overall	0.9995	0.9975	0.9975	0.9975

Table 3
Performance evaluation metrics for the one-channel CNN.

Class	Accuracy	Precision	Recall	F1 score
Normal	0.9269	0.5551	0.9856	0.7102
SGTL	0.9690	0.7650	0.9511	0.8479
CHRG	0.9746	0.9669	0.7467	0.8426
LTDN	0.9960	1.0000	0.9556	0.9773
CDS	0.9888	0.9901	0.8856	0.9349
POSRV	0.9925	1.0000	0.9178	0.9571
RMW	0.9978	0.9989	0.9767	0.9876
CWS	0.9762	1.0000	0.7378	0.8491
MSIV	0.9980	1.0000	0.9778	0.9888
RCP	0.9881	1.0000	0.8689	0.9298
MSS	0.9738	0.9052	0.7956	0.8468
Overall	0.9801	0.9256	0.8908	0.8975

Table 4
Performance evaluation metrics for the ANN.

Class	Accuracy	Precision	Recall	F1 score
Normal	0.8241	0.3344	0.9433	0.4937
SGTL	0.9346	0.6891	0.5122	0.5876
CHRG	0.9601	0.9485	0.5933	0.7300
LTDN	0.9886	0.9852	0.8878	0.9340
CDS	0.9882	0.9975	0.8722	0.9306
POSRV	0.9858	0.9987	0.8444	0.9151
RMW	0.9853	0.9446	0.8900	0.9165
CWS	0.9667	0.9948	0.6367	0.7764
MSIV	0.9854	0.9029	0.9400	0.9211
RCP	0.9866	0.9936	0.8578	0.9207
MSS	0.9525	0.8402	0.5900	0.6932
Overall	0.9598	0.8754	0.7789	0.8017

Table 5
Performance evaluation metrics for the PCA+GRU.

Class	Accuracy	Precision	Recall	F1 score
Normal	0.9976	0.9753	0.9987	0.9868
SGTL	0.9970	0.9690	0.9987	0.9836
CHRG	0.9968	0.9986	0.9667	0.9824
LTDN	1.0000	1.0000	1.0000	1.0000
CDS	0.9999	0.9987	1.0000	0.9993
POSRV	0.9998	1.0000	0.9973	0.9987
RMW	0.9999	1.0000	0.9987	0.9993
CWS	0.9972	1.0000	0.9693	0.9844
MSIV	1.0000	1.0000	1.0000	1.0000
RCP	0.9992	0.9908	1.0000	0.9954
MSS	0.9999	0.9987	1.0000	0.9993
Overall	0.9988	0.9937	0.9936	0.9936

we used only 10% of randomly sampled data from the training dataset apart from the test dataset. We implemented all classification models and the two-channel 2D image transformation method in a Python 3.6 environment with Keras and scikit-learn modules. We utilised four GPUs for multi-GPU computing in the training process and set the batch size to 128 for each training epoch in the neural network models.

Tables 2–6 present the performance evaluation results of the developed model and the four other major models, respectively. Overall, it is noteworthy that the developed two-channel CNN model shows far better performance in all performance evaluation metrics compared to the other classification models, except the PCA+GRU approach. While the results of the ANN and SVM approaches represent an average of nearly 96% accuracy, their precision, recall, and F1 scores were relatively low with large variances as compared to the CNN-based or GRU-based approaches. That is, ANN and SVM can generate volatile and biased classification results. Although the one-channel CNN had a decent level of classification accuracy, it showed lower performance in the classification of the normal state than the abnormal states, which is likely to result in a type 1 error in NPP abnormality diagnosis. On the other hand, while demonstrating superior performance compared to other classification models, the PCA+GRU approach showed a slightly lower level of performance in every evaluation metric than the developed two-channel CNN model. In spite of its similar performance though, the PCA+GRU approach takes considerable time to conduct PCA, and thus it is less time-efficient. In summary, given that the F1 scores for the developed model are at or close to 1 with little variation between them, we can confirm that the two-channel CNN model achieved a near-perfect performance as well as unbiased classification results.

The performance may vary with the context of analysis. For this reason, we conducted two additional tests using different time-lag values and different output variables to assess the robustness of the developed model. In the first test, time-lag values were increased from 5 s to 10 s and 20 s; Table 7 exhibits the performance evaluation results. The developed model provided the best performance when the time-lag was set to 20 s. Such results seem to come from the fact that the model might capture more information about changes in the plant parameters during longer time-lag value compared to the shorter time-lag value, although the number of data samples obtained by setting the time-lag to 5 s (82,500 samples) was greater than by setting the

Table 6
Performance evaluation metrics for the SVM (10% sampling).

Class	Accuracy	Precision	Recall	F1 score
Normal	0.9079	0.4960	0.8222	0.6187
SGTL	0.9661	0.8169	0.8078	0.8123
CHRG	0.8795	0.3904	0.5800	0.4667
LTDN	0.9745	0.9538	0.7567	0.8439
CDS	0.9836	0.9446	0.8711	0.9064
POSRV	0.9932	0.9988	0.9267	0.9614
RMW	0.9898	0.9385	0.9500	0.9442
CWS	0.9688	1.0000	0.6567	0.7928
MSIV	0.9809	0.8684	0.9311	0.8987
RCP	0.9525	0.8909	0.5444	0.6759
MSS	0.9712	0.8917	0.7778	0.8309
Overall	0.9607	0.8355	0.7840	0.7956

Table 7
Performance evaluation metrics for the developed two-channel CNN model with different time-lag values.

	5 s	10 s	20 s
Accuracy	0.9995	0.9999	1.0000
Precision	0.9975	0.9994	1.0000
Recall	0.9975	0.9994	1.0000
F1 score	0.9975	0.9994	1.0000

Table 8
Performance evaluation metrics for the developed two-channel CNN model with 19 sub-procedures (time-lag = 5 s).

Class	Accuracy	Precision	Recall	F1 score
Normal	0.9994	0.9894	1.0000	0.9947
SGTL	0.9998	0.9987	0.9973	0.9980
CHRG [LN]	0.9997	0.9987	0.9960	0.9973
CHRG [PM]	0.9999	0.9973	1.0000	0.9987
CHRG [VV]	0.9999	0.9987	1.0000	0.9993
LTDN [LN]	1.0000	1.0000	1.0000	1.0000
LTDN [VV]	1.0000	1.0000	1.0000	1.0000
CDS	1.0000	1.0000	1.0000	1.0000
POSRV	1.0000	1.0000	1.0000	1.0000
RMW [LL]	0.9997	1.0000	0.9947	0.9973
RMW [LH]	1.0000	1.0000	1.0000	1.0000
CWS [LN]	1.0000	1.0000	1.0000	1.0000
CWS [VV]	1.0000	1.0000	1.0000	1.0000
CWS [PM]	1.0000	1.0000	1.0000	1.0000
MSIV	1.0000	1.0000	1.0000	1.0000
RCP [LC]	0.9997	1.0000	0.9947	0.9973
RCP [SD]	1.0000	1.0000	1.0000	1.0000
MSS [VV]	1.0000	1.0000	1.0000	1.0000
MSS [LN]	1.0000	1.0000	1.0000	1.0000
Overall	0.9999	0.9991	0.9991	0.9991

time-lag to 20 s (33,000 samples). In addition, it should be noted that although the performance of the developed model with a 5 s time-lag was slightly lower than those with 10 and 20 s time-lags, results demonstrate that almost all samples were classified into the correct abnormal states even with the 5 s time-lag. In other words, we can conclude that the developed model is robust across different time-lag values.

In the second test, considering that each abnormal event includes multiple sub-procedures representing different causes for the given abnormal event, we tested the two-channel CNN again using a total of 19 sub-procedures as its output values; Table 8 gives the performance evaluation results of this test. Although the precision deteriorated slightly in the classification of the normal state, results in general show that the developed model achieved adequate performance in the classification of the 19 sub-procedures. In summary, the results of the robustness tests indicate that the developed two-channel CNN model is robust across different contexts of analysis, including time-efficient abnormality diagnosis as well as the ability to handle up to dozens of abnormal events.

6. Discussion

To be applied to a real NPP system and give practical assistance to operators, any abnormality diagnostic model must have the ability to classify abnormal events and the normal state in real-time with high reliability. Regarding the abnormality diagnosis as a classification problem, the reliability can be defined as the highest probability that the model predicted among the outputs. However, the results of our experiments were limited to classification using a dataset prepared beforehand, so a problem remains as to whether the performance of the developed model can be maintained during real-time diagnosis or not. Moreover, our experiments examined classification performance only without any measure of the reliability of the results showing how confident the model provides classification results.

To better examine the practicality of the developed model, we conducted additional experiments that assessed the performance of the pre-trained two-channel CNN model and the reliability of its classification results for longer NPP simulator operating data. To this end, we additionally collected 3 min of scenario data that were not utilised in the model training or performance evaluation, and let the developed CNN model diagnose the abnormal events of the newly collected scenarios. The results of the additional experiment demonstrated that the model was able to almost perfectly diagnose the abnormal events for the new samples containing scenario data after 30 s of simulation; Fig. 7 presents some of the results as graphs of the reliability for the additional 3 min scenario samples, where each line corresponds to the reliability value of each NPP state predicted by the model. In Fig. 7(a), which shows the prediction result for the normal sample, the model has almost correctly diagnosed the normal state, but has confused the normal state with the RCP abnormal event over the range of 50 s to 75 s. One possible cause of this confusion is the scope of the training data, which was limited to 30 s after the simulation started. For example, the trend of the normal state and the RCP abnormal event may be similar in the range of 50 s to 75 s. At this point, the model will diagnose based on existing trends learned from the data earlier than 30 s only, which can confuse these two states. On the other hand, Fig. 7(b)–(d) represent the prediction results for the POSRV, CHRG, and RMW samples, respectively. In the three graphs, the model almost perfectly diagnosed each abnormal event with at least 80% reliability over the entire time period. Overall, with relatively high reliability, the developed two-channel CNN model correctly diagnosed the abnormal events and normal state for the scenario data after 30 s. Thus, the results of this additional experiment confirm that the developed model has the potential to be used as an operator support system for real-time abnormality diagnosis in the real NPP systems. Of course, this experiment does not guarantee that the developed model will show stable performance for a variety of situations not covered in this study. For example, for NPP operation at less than 100% power generation, the normal state can be misclassified as abnormal. Moreover, it is also possible that the model doubts the normal state in some cases, as exemplified in Fig. 7(a). In this context, to further improve the robustness of the developed model for real-time diagnosis, we need to collect additional data related to such different situations for further model training in future studies.

7. Conclusion

This study developed a convolutional neural network model for abnormality diagnosis in NPPs. The main principle is that CNNs with their ability to deal with image data can be effective in handling the massive amount of data generated in real time in an NPP [38]. With this consideration, the proposed approach adopts two-channel 2D images: one channel represents

(a) Normal state

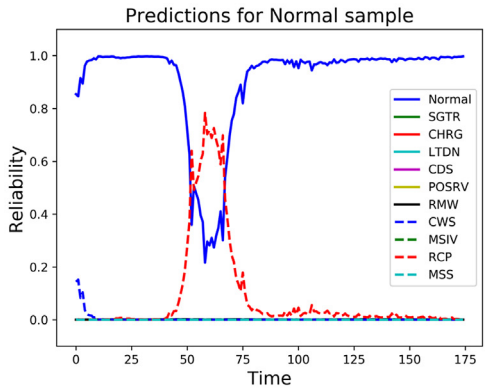

(b) Abnormal event POSRV

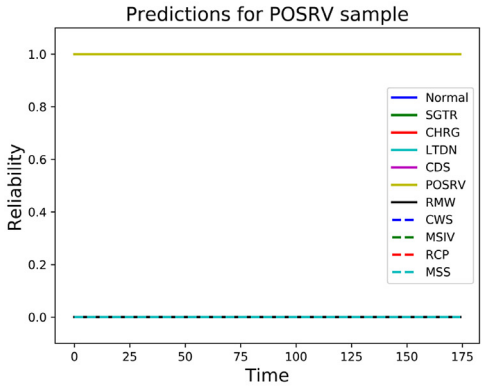

(c) Abnormal event CHRG

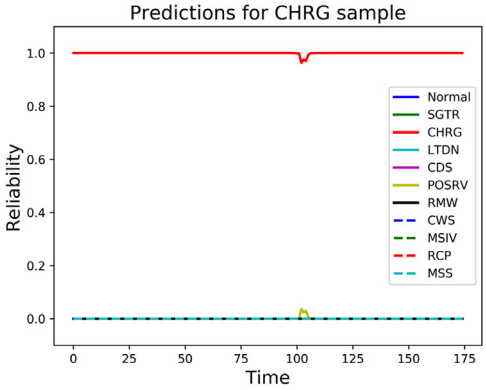

(d) Abnormal event RMW

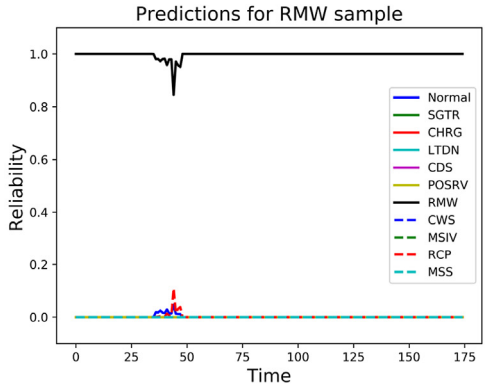

Fig. 7. Graphs of reliability for the predicted NPP states along time (a) Normal state (b) Abnormal event POSRV (c) Abnormal event CHRG (d) Abnormal event RMW.

the current NPP state values, and the other channel represents the changing patterns of the values over a prescribed time period.

Experimental results from a full-scope simulator confirmed that the developed two-channel CNN model outperforms other classification models in terms of accuracy and reliability. The developed model showed almost perfect performance, especially with a 20 s time-lag, and it was also found to be robust according to different analysis contexts. Moreover, the additional experiment demonstrated the great ability of our approach for online diagnosis of abnormal events. Therefore, the developed two-channel CNN model is expected to serve as a real-time operator supporting system to reduce the time and effort associated with abnormality diagnosis in NPPs.

Despite the confirmed validation, this study has limitations that should be addressed by future research. First, this study relies only on the data generated by the simulator, although it is considered reliable and the developed model can be deployed in practice without any further training or modification. However, the performance of the model should be assessed by using the data obtained from the real NPP systems since safety is given as the top priority and any misclassification may lead to huge public and economic loss. Second, only 10 abnormal events were considered among 82 possible events, although they were related to various components across the plant. Further testing on different types of abnormal events is essential to confirm the validity of the two-channel CNN model. Third, the proposed approach only focused on diagnosing abnormal events in an NPP, and thus is not intended to provide information about the proper corrective actions to be performed. The current predictive approach should thus be extended to prescriptive approaches, for which reinforcement learning techniques could be useful. Finally, the developed model was not trained to handle multiple abnormal events in one scenario or answer "don't know" for an untrained scenario. In real NPP systems, once abnormal behaviour is detected, more than one abnormal event often occurs at the same time. In such situations, operators need to make a quick and accurate judgement as to the cause of the abnormality. Thus, the proposed model, as an operator support system for real-time abnormality diagnosis, must actively consider these issues. In future research, they are expected to be solved by changing the output of the model as follows. By employing a sigmoid instead of softmax as the activation function, the model could predict a value between 0 and 1 for each class, and thus the output can be regarded as individual reliability for each normal or abnormal event. Accordingly, the model will be able to perform multi-label classification by setting thresholds for predictions, such as 0.5. In this context, for data samples in which the model predicts values above the threshold for two or more classes, they will be judged to be multiple abnormal events. On the other hand, for other data samples in which the model predicts values below the threshold for every class, they will be labelled as "don't know".

CRediT authorship contribution statement

Gyumin Lee: Data curation, Methodology, Software, Writing - original draft, Writing - review & editing. **Seung Jun Lee:** Conceptualization, Data curation, Writing - original draft, Writing - review & editing, Supervision. **Changyong Lee:** Conceptualization, Methodology, Writing - original draft, Writing - review & editing, Supervision.

Declaration of competing interest

The authors declare that they have no known competing financial interests or personal relationships that could have appeared to influence the work reported in this paper.

Acknowledgements

This work was supported by the Korea Institute of Energy Technology Evaluation and Planning (KETEP) and the Ministry of Trade, Industry & Energy (MOTIE) of the Republic of Korea (No. 20171510102040).

Appendix A. Supplementary data

Supplementary material related to this article can be found online at https://doi.org/10.1016/j.asoc.2020.106874.

References

[1] M.J. Embrechts, S. Benedek, Hybrid identification of nuclear power plant transients with artificial neural networks, IEEE Trans. Ind. Electron. 51 (3) (2004) 686–693.
[2] M.H. Hsieh, S.L. Hwang, K.H. Liu, S.F.M. Liang, C.F. Chuang, A decision support system for identifying abnormal operating procedures in a nuclear power plant, Nucl. Eng. Des. 249 (2012) 413–418.
[3] S.J. Lee, P.H. Seong, A dynamic neural network based accident diagnosis advisory system for nuclear power plants, Prog. Nucl. Energy 46 (3–4) (2005) 268–281.
[4] J. Park, W. Jung, A systematic framework to investigate the coverage of abnormal operating procedures in nuclear power plants, Reliab. Eng. Syst. Saf. 138 (2015) 21–30.
[5] J.S. Ha, P.H. Seong, M.S. Lee, J.H. Hong, Development of human performance measures for human factors validation in the advanced MCR of APR-1400, IEEE Trans. Nucl. Sci. 54 (6) (2007) 2687–2700.
[6] Y. Yao, J. Wang, M. Xie, L. Hu, J. Wang, A new approach for fault diagnosis with full-scope simulator based on state information imaging in nuclear power plant, Ann. Nucl. Energy 141 (2020) 107274.
[7] H. Wang, M.J. Peng, J.W. Hines, G.Y. Zheng, Y.K. Liu, B.R. Upadhyaya, A hybrid fault diagnosis methodology with support vector machine and improved particle swarm optimization for nuclear power plants, ISA Trans. 95 (2019) 358–371.
[8] S. Tolo, X. Tian, N. Bausch, V. Becerra, T.V. Santhosh, G. Vinod, E. Patelli, Robust on-line diagnosis tool for the early accident detection in nuclear power plants, Reliab. Eng. Syst. Saf. 186 (2019) 110–119.
[9] V.H.C. Pinheiro, M.C. dos Santos, F.S.M. do Desterro, R. Schirru, C.M.D.N.A. Pereira, Nuclear Power Plant accident identification system with don't know response capability: Novel deep learning-based approaches, Ann. Nucl. Energy 137 (2020) 107111.
[10] K. Nabeshima, T. Suzudo, K. Suzuki, E. Türkcan, Real-time nuclear power plant monitoring with neural network, J. Nucl. Sci. Technol. 35 (2) (1998) 93–100.
[11] A. Krizhevsky, I. Sutskever, G.E. Hinton, Imagenet classification with deep convolutional neural networks, in: Advances in Neural Information Processing Systems, 2012, pp. 1097–1105.
[12] S. Chaudhry, R. Chandra, Face detection and recognition in an unconstrained environment for mobile visual assistive system, Appl. Soft Comput. 53 (2017) 168–180.
[13] H. Li, Z. Lin, X. Shen, J. Brandt, G. Hua, A convolutional neural network cascade for face detection, in: Proceedings of the IEEE Conference on Computer Vision and Pattern Recognition, 2015, pp. 5325–5334.
[14] D.C. Ciresan, U. Meier, L.M. Gambardella, J. Schmidhuber, Convolutional neural network committees for handwritten character classification, in: 2011 International Conference on Document Analysis and Recognition, IEEE, 2011, pp. 1135–1139.
[15] A. Garcia-Garcia, S. Orts-Escolano, S. Oprea, V. Villena-Martinez, P. Martinez-Gonzalez, J. Garcia-Rodriguez, A survey on deep learning techniques for image and video semantic segmentation, Appl. Soft Comput. 70 (2018) 41–65.
[16] Q. Li, W. Cai, X. Wang, Y. Zhou, D.D. Feng, M. Chen, Medical image classification with convolutional neural network, in: 2014 13th International Conference on Control Automation Robotics and Vision (ICARCV), 2014, pp. 844–848.
[17] Y. Wang, Y. Chen, N. Yang, L. Zheng, N. Dey, A.S. Ashour, …, F. Shi, Classification of mice hepatic granuloma microscopic images based on a deep convolutional neural network, Appl. Soft Comput. 74 (2019) 40–50.
[18] M.S. Lee, J.H. Hong, J.K. Suh, S.H. Lee, D.H. Hwang, Development of human factors validation system for the advanced control room of APR1400, J. Nucl. Sci. Technol. 46 (1) (2009) 90–101.
[19] J. Park, W. Jung, J. Ha, Y. Shin, Analysis of operators' performance under emergencies using a training simulator of the nuclear power plant, Reliab. Eng. Syst. Saf. 83 (2) (2004) 179–186.

[20] R. Guide, Standard Format and Content of Safety Analysis Reports for Nuclear Power Plants, US Nuclear Regulatory Commission, Washington, DC, 1978.
[21] J.J. Gertler, Survey of model-based failure detection and isolation in complex plants, IEEE Control Syst. Mag. 8 (6) (1988) 3–11.
[22] R. Isermann, Fault-Diagnosis Systems: An Introduction from Fault Detection to Fault Tolerance, Springer Science and Business Media, 2006.
[23] K.C. Gross, R.M. Singer, S.W. Wegerich, J.P. Herzog, R. VanAlstine, F. Bockhorst, Application of a Model-Based Fault Detection System to Nuclear Plant Signals, Argonne National Lab., IL (United States), 1997.
[24] R. Razavi-Far, H. Davilu, V. Palade, C. Lucas, Model-based fault detection and isolation of a steam generator using neuro-fuzzy networks, Neurocomputing 72 (13–15) (2009) 2939–2951.
[25] S. Mandal, N. Sairam, S. Sridhar, P. Swaminathan, Nuclear power plant sensor fault detection using singular value decomposition-based method, Sādhanā 42 (9) (2017) 1473–1480.
[26] J. Ma, J. Jiang, Applications of fault detection and diagnosis methods in nuclear power plants: A review, Prog. Nucl. Energy 53 (3) (2011) 255–266.
[27] M. Horiguchi, N. Fukawa, K. Nishimura, Development of nuclear power plant diagnosis technique using neural networks, in: Proceedings of the First International Forum on Applications of Neural Networks to Power Systems, IEEE, 1991, pp. 279–282.
[28] T.V. Santosh, G. Vinod, R.K. Saraf, A.K. Ghosh, H.S. Kushwaha, Application of artificial neural networks to nuclear power plant transient diagnosis, Reliab. Eng. Syst. Saf. 92 (10) (2007) 1468–1472.
[29] E. Zio, A support vector machine integrated system for the classification of operation anomalies in nuclear components and systems, Reliab. Eng. Syst. Saf. 92 (5) (2007) 593–600.
[30] J. Galbally, D. Galbally, A pattern recognition approach based on DTW for automatic transient identification in nuclear power plants, Ann. Nucl. Energy 81 (2015) 287–300.
[31] A. Ayodeji, Y.K. Liu, H. Xia, Knowledge base operator support system for nuclear power plant fault diagnosis, Prog. Nucl. Energy 105 (2018) 42–50.
[32] B.S. Peng, H. Xia, Y.K. Liu, B. Yang, D. Guo, S.M. Zhu, Research on intelligent fault diagnosis method for nuclear power plant based on correlation analysis and deep belief network, Prog. Nucl. Energy 108 (2018) 419–427.
[33] J.M. Kim, G. Lee, C. Lee, S.J. Lee, Abnormality diagnosis model for nuclear power plants using two-stage gated recurrent units, Nucl. Eng. Technol. (2020).
[34] A. dos Santos Nicolau, R. Schirru, A new methodology for diagnosis system with 'Don't Know'response for Nuclear Power Plant, Ann. Nucl. Energy 100 (2017) 91–97.
[35] M. Sudhakar, J.A. Mayan, N. Srinivasan, Intelligent data prediction system using data mining and neural networks, in: Proceedings of the International Conference on Soft Computing Systems, 2016, pp. 489–500.
[36] T.G. Van Niel, T.R. McVicar, B. Datt, On the relationship between training sample size and data dimensionality: Monte Carlo analysis of broadband multi-temporal classification, Remote Sens. Environ. 98 (4) (2005) 468–480, 593-600.
[37] S.J. Chang, J.B. Park, Wire mismatch detection using a Convolutional Neural Network and Fault localization based on Time–Frequency-Domain Reflectometry, IEEE Trans. Ind. Electron. 66 (3) (2018) 2102–2110.
[38] O.B. Sezer, A.M. Ozbayoglu, Algorithmic financial trading with deep convolutional neural networks: Time series to image conversion approach, Appl. Soft Comput. 70 (2018) 525–538.
[39] L. Wen, X. Li, L. Gao, Y. Zhang, A new convolutional neural network-based data-driven fault diagnosis method, IEEE Trans. Ind. Electron. 65 (7) (2017) 5990–5998.
[40] 3KEYMASTER Simulator 2013, Western Service Corporation, Frederick, MD, USA.
[41] C. Clark, A. Storkey, Training deep convolutional neural networks to play go, in: International Conference on Machine Learning, 2015, pp. 1766–1774.
[42] J.D. Hunter, Matplotlib: A 2D graphics environment, Comput. Sci. Eng. 9 (3) (2007) 90–95.
[43] B. Zhou, A. Khosla, A. Lapedriza, A. Oliva, A. Torralba, Learning deep features for discriminative localization, in: Proceedings of the IEEE Conference on Computer Vision and Pattern Recognition, 2016, pp. 2921–2929.
[44] C. Lee, O. Kwon, M. Kim, D. Kwon, Early identification of emerging technologies: A machine learning approach using multiple patent indicators, Technol. Forecast. Soc. Change 127 (2018) 291–303.
[45] M. Sokolova, G. Lapalme, A systematic analysis of performance measures for classification tasks, Inf. Process. Manage. 45 (4) (2009) 427–437.
[46] C. Lee, S. Jo, D. Kwon, M. Pecht, Capacity-fading behavior analysis for early detection of unhealthy Li-ion Batteries, IEEE Trans. Ind. Electron. (2020) http://dx.doi.org/10.1109/TIE.2020.2972468.
[47] American Nuclear Society Standards Committee, Nuclear Power Plant Simulators for Use in Operator Training and License Examination, ANSI/ANS 3.5, American Nuclear Society, 1998.
[48] A. Ignatov, Real-time human activity recognition from accelerometer data using Convolutional Neural Networks, Appl. Soft Comput. 62 (2018) 915–922.
[49] D.P. Kingma, J. Ba, Adam: A method for stochastic optimization, 2014, arXiv preprint, arXiv:1412.6980.
[50] Y. LeCun, Y. Bengio, G. Hinton, Deep learning, Nature 521 (7553) (2015) 436.
[51] M.G. Na, W.S. Park, D.H. Lim, Detection and diagnostics of loss of coolant accidents using support vector machines, IEEE Trans. Nucl. Sci. 55 (1) (2008) 628–636.